Int J Thermophys (2008) 29:2072–2087
DOI 10.1007/s10765-008-0378-0

Determination of Transient Thermal Interface Resistance Between Two Bonded Metal Bodies using the Laser-Flash Method

N. D. Milošević

Published online: 20 February 2008

Abstract The paper presents the data reduction analysis for measurements of the transient thermal interface resistance between two bonded metal bodies using the laser-flash method. By using two different mathematical models, i.e., a two-layered and a three-layered model, whose complete analytical solutions for realistic conditions are provided, different results for final values and their uncertainties can be obtained. The analysis has been applied to experimental data measured from samples prepared with three different bonding materials, cyanoacrylate, metal epoxy resin, and silicone rubber.

Keywords Adhesive properties · Laser-flash method · Multilayered heat conduction · Multilayered materials · Parameter estimation · Thermal contact resistance · Thermal interface resistance

1 Introduction

There is a constant and significant increase of the use of multilayered systems in research and industry, and an important part of these applications relates to the heat conduction over metallic bodies in contact. Whether mechanically connected or bonded by various adhesive agents, such systems always result in inferior properties regarding the heat conduction in comparison to those without contact. A quantitative description of such behavior is represented by the value of the thermal contact resistance (TCR) when the bodies are in pure mechanical contact or by the value of the thermal interface resistance (TIR) when the bodies are connected in addition by some thin intermediate material. While the first property depends only on the macro- and microscopic

N. D. Milošević (✉)
"Vinča" Institute of Nuclear Sciences, P.O. Box 522, 11001 Belgrade, Serbia
e-mail: nenadm@vin.bg.ac.yu

qualities of touching surfaces and the contact pressure and temperature, the latter one depends on the physical properties of the intermediate layer as well. The values of TCR and TIR, especially the first one, may also depend on the heat conduction regime, i.e., whether they are measured in a steady or transient state of heat conduction [1].

One of the several experimental methods used for TCR and TIR determination is the transient laser-flash method. This method was originally used for measuring the thermal diffusivity of solid homogeneous materials [2], but its application can be easily extended for transient TCR and TIR measurements of layered materials. Such use was first proposed by Laurent et al. [3], who derived a simple formula for the computation of TCR from experimental data. Somewhat later, their procedure was theoretically developed by Degiovanni et al. [4] who gave the general analytical solution for multilayer structures, but applied only the two-layered model (2LM) for TCR determination. Independently, Lee [5] derived two- and three-layer solutions for TCR and TIR measurements, taking into account the finite pulse effect, but neglecting the influence of heat loss. Using the two-layered model, Inoue and Ohmura [6] contributed to TCR measurements with related error analysis, while more recently Dusza [7], Griesinger et al. [8], and Milošević et al. [9] proposed parameter estimation techniques for related data reduction.

On the other side, using the three-layered model (3LM) and the analytical solution derived by Lee [5], Campbell et al. [10] and Hasselman et al. [11] measured the TCR between different adhesives and Si, Al, and AlSiC platelets, while Bai et al. [12] determined the TCR of different copper-solder-copper specimens. However, the measurement of TCR by using the 3LM and the laser-flash method is far more complex than in the case of the 2LM. First, the physical properties of the intermediate layer must be well known, especially the properties such as the thermal conductivity or thermal diffusivity whose uncertainties may significantly influence the final results. An independent evaluation of these properties may be another complex experiment. Second, the values of independently measured properties of free-standing intermediate material may not be equivalent to those of the same material in a bonded system. Different conditions, such as the processing and curing period, temperature and pressure, thickness, area, and shape of the intermediate layer, as well as the components of the material used, may influence the thermal conductivity and thermal diffusivity of the intermediate layer and result in considerable changes in their initial values. Finally, in transient heat conduction, the TCR at two contact surfaces cannot be computed as a simple difference of the total thermal resistance between two bonded bodies and the thermal resistance of the intermediate layer because such a formula is valid only in the steady-state regime. Because of all these reasons, if one applies the 3LM, the laser-flash method is much more appropriate for the transient TIR than for the TCR measurements.

This work, therefore, investigates the possibilities of transient TIR measurements by using the laser-flash method and two different mathematical models. As the TIR corresponds to a thermal resistance made by an intermediate layer and thermal contact resistances between the intermediate and outside layers, the sample structure is three layered in reality. However, for very thin intermediate layers, the structure can be considered as two layered as well, which reduces significantly the processing time. The differences between these models and consequences on final results are consid-

ered with several experimental examples. As the application of well-defined highly conductive metallic layers is the most appropriate for measurements of the transient TCR using the laser-flash method [9], experiments in this research were performed on samples made from high-purity copper disks.

2 Theory

The principle of the laser-flash method is simple: the energy of a short laser pulse is absorbed at one surface of a thin disk-shaped sample and at the same time, the temperature evolution of the other sample side is recorded. A subsequent analysis of this signal leads to the thermal diffusivity of the sample material.

The same principle is applied in the case of composite or multilayer materials, but the related temperature evolution is a more complex function of the involved physical properties. In addition to the influence of thermal contact resistances between layers, the influence of thermal diffusivity, specific heat capacity, and density of each layer must also be considered.

In the case of two bonded layers, there are two ways for forming an appropriate physical model: (a) when the adhesive material is considered as a simple contact between the surfaces of bonded materials and (b) when the adhesive material acts as another layer. The first is a two-layered (2LM) model, while the second is a three-layered model (3LM).

2.1 Mathematical Models

In the case of one-dimensional (1D) transient heat conduction, the two mathematical models are based on referential systems as shown in Fig. 1. The bonded layers are described by several properties, such as thermal diffusivity a, heat capacity at constant pressure c, mass density ρ, and thickness L. In the 2LM case, the intermediate layer is represented by a single thermal contact resistance R_c, while in the 3LM, by corresponding physical properties a_i, c_i, ρ_i, and L_i and by two thermal contact resistances R_{c1} and R_{c2}, which correspond to the pure contact between the layers. Free surfaces of both systems are described by the related heat transfer coefficient h. The front surface of the system absorbs, from $t = 0$ to $t = \tau$, the total energy per square meter Q. The pulse duration τ is much smaller than the characteristic time of the heat diffusion through the sample.

Having the Fourier law and the conservation of energy principles and assuming that the absolute temperature variation of the system is not significant in the sense that thermophysical properties of used materials remain constant, the transient temperature of any layer of the above systems can be expressed by a well-known heat diffusion partial differential equation. In the laser-flash method, only the transient temperature change T of the back free surface is of interest and its analytical solution for both 2LM and 3LM can be found by using the separation of variables technique and proper boundary and initial conditions (see Refs. [13,14], for example).

If one assumes that the absorption depth of the energy Q is much smaller than the thickness L_1, which is practically always true for metals, the temperature change T

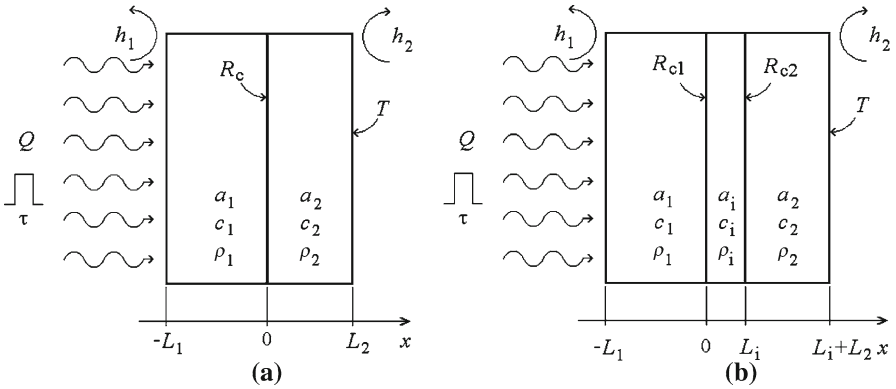

Fig. 1 Physical models for two bonded materials with an intermediate layer treated with (**a**) a negligible thickness (2LM) and (**b**) a finite thickness (3LM)

for the 2LM given in Fig. 1a and for time $t > \tau$ can be computed from the following expression:

$$T^{(2\mathrm{LM})} = \frac{Q}{\rho_1 c_1 \tau}\sqrt{\frac{a_1}{a_2}}\sum_{n=1}^{+\infty}\frac{1}{\beta_n^2 A_n}\left(\sin\varphi_{1n} + s_{1n}\cos\varphi_{1n}\right) \times \left(-\sin\varphi_{2n} + s_{2n}\cos\varphi_{2n}\right)\left(\mathrm{e}^{\beta_n^2\tau} - 1\right)\mathrm{e}^{-\beta_n^2 t} \tag{1}$$

where the functions $A_n, s_{1n}, s_{2n}, \varphi_{1n}$, and φ_{2n} are given by Eqs. A1–A4 in the Appendix and parameters k_1 and k_2 are the related thermal conductivities of the two layers ($k = \rho ca$). Positive numbers β_n represent eigenvalues of the solution, and they can be found by the efficient and reliable "sign-count" method proposed by Mikhailov and Vulchanov [15]. According to that procedure, the number of eigenvalues $N(\beta_0, S)$ below an arbitrary value β_0 is equal to

$$N(\beta_0, S) = \mathrm{int}\left(\frac{\phi_{01}}{\pi}\right) + \mathrm{int}\left(\frac{\phi_{02}}{\pi}\right) + N\left[S(\beta_0)\right] \tag{2}$$

where $N[S(\beta_0)]$ is the number of negative elements of the set $S(\beta_0) = \{d_1,\ d_2,\ d_3,\ d_4\}$, defined by Eqs. A5–A9 given in the Appendix. If one varies the value β_0 by using Eq. 2 and uses the principle of dichotomy, the determination of eigenvalues β_n is straightforward. The number of eigenvalues β_n needed for the computation of Eq. 1 depends on the solution convergence and the required accuracy.

In the case of the 3LM (Fig. 1b), assuming the same absorption depth as above, the temperature change T for the time $t > \tau$ can be written as

$$T^{(3\mathrm{LM})} = 2\frac{Q}{\tau}\frac{\rho_2 c_2}{\rho_1 c_1}\sum_{n=1}^{+\infty}\frac{p_{5n}}{\beta_n^2 A_n}\left(-\sin\varphi_{1n} + p_{1n}\cos\varphi_{1n}\right) \times \left[\sin\left(\varphi'_{\mathrm{i}n} + \varphi_{2n}\right) + p_{4n}\cos\left(\varphi'_{\mathrm{i}n} + \varphi_{2n}\right)\right]\left(\mathrm{e}^{\beta_n^2\tau} - 1\right)\mathrm{e}^{-\beta_n^2 t} \tag{3}$$

where the functions A_n, p_{1n} to p_{5n}, φ_{in}, and φ'_{in} are given by Eqs. A10–A16 in the Appendix. The eigenvalues β_n for this case can be found by using the same method as above, but from Eq. 4, where $N[S(\beta_0)]$ is the number of negative elements of the set $S(\beta_0) = \{g_1,\ g_2,\ g_3,\ g_4\}$, defined by Eqs. A17–A23.

$$N(\beta_0, S) = \text{int}\left(\frac{\varphi_{01}}{\pi}\right) + \text{int}\left(\frac{\varphi_{0\text{i}}}{\pi}\right) + \text{int}\left(\frac{\varphi_{02}}{\pi}\right) + N\left[S(\beta_0)\right] \tag{4}$$

To derive desired parameters from the experimental data, the solution of the theoretical model is applied in a corresponding parameter estimation procedure.

2.2 Applied Estimation Procedure and Related Uncertainties

For the case of nonlinear estimation, when sensitivity coefficients are the functions of proper parameters and probability functions are by experience or by assumption Gaussian, the well-known Gauss parameter estimation method is most frequently used and its general description can be found in Beck and Arnold [16].

In this work, the so called maximum likelihood estimator has been applied, i.e., where the Gauss linearized iterative equation has the following form [16]:

$$\mathbf{b}^{(k+1)} = \mathbf{b}^{(k)} + \left[\mathbf{X}^{\text{t}(k)}\mathbf{W}^{-1}\mathbf{X}^{(k)}\right]^{-1}\mathbf{X}^{\text{t}(k)}\mathbf{W}^{-1}\left[\mathbf{Y} - \mathbf{T}^{(k)}(\mathbf{b}^{(k)})\right] \tag{5}$$

where $\mathbf{T}$ is the matrix of computed values from the model $[m \times 1]$, $\mathbf{Y}$ is the matrix of measured values $[m \times 1]$, $\mathbf{b}$ is the matrix of parameters for estimation $[p \times 1]$, $\mathbf{X}$ is the matrix of sensitivity coefficients of parameters for estimation $[m \times p]$, and $\mathbf{W}$ is the variance–covariance matrix of measured values $[m \times m]$. Diagonal elements of the matrix $\mathbf{W}$ are the variances of measured values, σ_j^2, where $j = 1, \ldots, m$, while the off-diagonal elements are their covariances. When the measured values are not correlated, the matrix $\mathbf{W}$ is purely diagonal. Numbers m and p are numbers of measured points and parameters for estimation, respectively.

The iterative Eq. 5 should be stopped when the convergence criterion is satisfied. The standard deviation of estimated parameters can be approximately found from the expression [16],

$$\mathbf{u}^{(\text{final})} \approx \sqrt{\text{diag}\left\{\left[\mathbf{X}^{\text{t}(\text{final})}\mathbf{W}^{-1}\mathbf{X}^{(\text{final})}\right]^{-1}\right\}} \tag{6}$$

In addition to the standard deviation of Eq. 6, for testing the quality of results, one could use the positive square root of the sum of squared normalized differences between measured and computed values, which is, in fact, the relative standard deviation of a fitted curve through the experimental data.

In the estimation procedure, only two parameters have been estimated simultaneously for both models: the TIR (i.e., R_c from the 2LM and a_eff from the 3LM, which will be defined in the next section) and the absorbed energy Q. All the other parameters

from Eqs. 1 and 3 have been assumed to be known: 11 parameters in the 2LM and 16 in the 3LM.

In practice, every known parameter introduces some uncertainty which may influence the accuracy of estimation results. The consideration of such influences can be very arduous and time consuming, especially in strongly nonlinear systems, which is the present case, where the influence of higher-order terms in the propagation of uncertainty law cannot be neglected. Consequently, the matrix **W** should possess diagonal and off-diagonal elements made by the summation of numerous combined partial derivatives of second and third order, but the computation of these functions, in practice, would take too much time.

Therefore, instead of considering the uncertainties of known parameters directly in the estimation procedure of Eq. 5, their influence has been analyzed in this work by changing the a priori values of known parameters in the range of their maximum uncertainties. In the 2LM, due to the small influence of their uncertainties, all the values of known parameters were assumed to be exact, i.e., with zero uncertainties. In the 3LM, however, the thickness, density, and specific heat capacity of the intermediate layer were taken to have some finite uncertainty and the estimations were carried out for each combination of the a priori values of known parameters.

2.3 Differences in Computed Temperatures by Two Models

In this research, the transient TIR has been used for estimation in both models. It is clear from Fig. 1 that the TIR corresponds to R_c in the 2LM. However, in the 3LM, the TIR is not a simple sum of three resistances in series, R_{c1}, R_{c2}, and $L_i/(a_i\rho_i c_i)$, because such addition is correct only in steady-state heat conduction. Instead, the TIR between the layers can be expressed by an effective transient thermal resistance, L_{eff}/k_{eff}, where k_{eff} is the effective thermal conductivity. In reality, $L_{eff} \approx L_i$, $\rho_{eff} \approx \rho_i$, and $c_{eff} \approx c_i$, so the TIR in the 3LM can be represented approximately by only one term, $L_i/(a_{ieff}\rho_i c_i)$, where a_{eff} is the effective thermal diffusivity. Then, in Eq. 3, R_{c1} and R_{c2} should be set to a very small value and a_i should be replaced to a_{eff}. Finally, the transient TIR for both models can be written as

$$\mathrm{TIR} = R_c \quad (2\mathrm{LM}) \tag{7}$$

$$\mathrm{TIR} \approx \frac{L_i}{a_{eff}\rho_i c_i} \quad (3\mathrm{LM}) \tag{8}$$

To compare the models, the differences between related temperatures have been analyzed for a specific set of parametric values given in Table 1. These values have been chosen according to known and assumed values of physical properties used in the experimental part of this research, where copper has been the bonded material and cyanoacrylate the adhesive. The properties have been selected in such a way that they describe almost an identical physical system: the thermal contact resistance R_c from

Table 1 Example of parametric values for the model comparison

Property	2LM	3LM
a_1, a_2 ($m^2 \cdot s^{-1}$)	1.19×10^{-4}	1.19×10^{-4}
c_1, c_2 ($J \cdot kg^{-1} \cdot K^{-1}$)	386	386
ρ_1, ρ_2 ($kg \cdot m^{-3}$)	8,960	8,960
L_1, L_2 (mm)	1	1
h_1, h_2 ($W \cdot m^{-2} \cdot K^{-1}$)	10	10
R_c ($m^2 \cdot K \cdot W^{-1}$)	10^{-5}; 10^{-4}; 10^{-3}; 10^{-2}	–
a_{eff} ($m^2 \cdot s^{-1}$)	–	10^{-7}
c_i ($J \cdot kg^{-1} \cdot K^{-1}$)	–	1,000
ρ_i ($kg \cdot m^{-3}$)	–	1,000
L_i(μm)	–	1; 10; 100; 1,000
R_{c1}, R_{c2} ($m^2 \cdot K \cdot W^{-1}$)	–	10^{-9}
Q ($J \cdot m^{-2}$)	100	100
τ (ms)	1	1

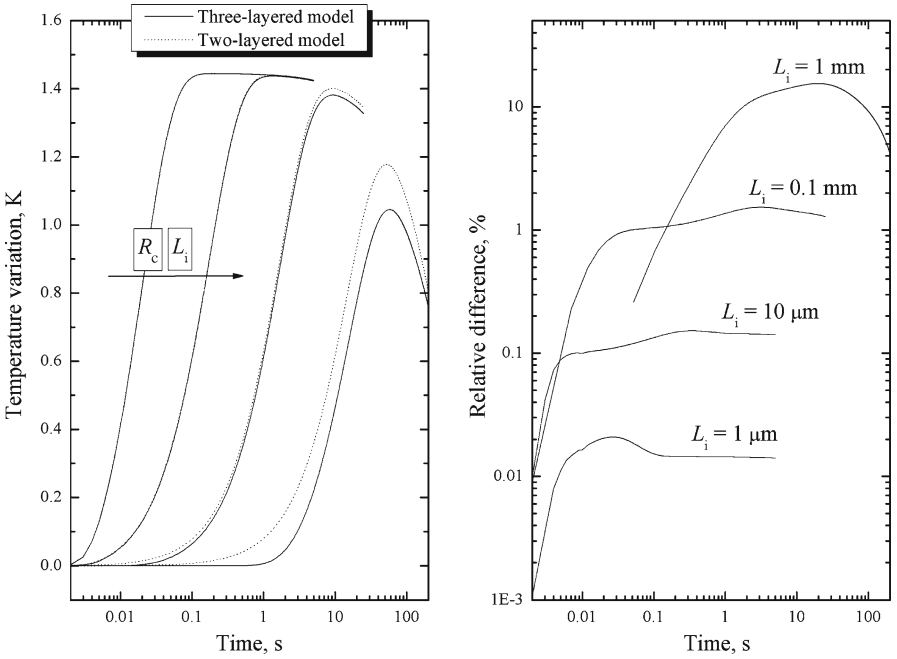

Fig. 2 Computed temperature evolutions and their differences for two mathematical models and for parametric values given in Table 1

2LM is equal to the ratio $L_i/(a_{eff}\rho_i c_i)$ from 3LM, and all other common parameters are identical.

The temperature evolutions computed from Eqs. 1 and 3 and their relative difference for the values given in Table 2 are presented in Fig. 2. In the first diagram, a significant time delay can be observed for both models, as expected. An increase of the parameters

R_c and L_i produces a corresponding increase of that delay, and for higher values of these parameters, distinctions between related temperatures become more important. So, in the second diagram, the relative differences between the temperatures can be seen. According to them, for a thickness of the intermediate layer of 0.1 mm, the temperature from the 2LM differs by about 1% from corresponding temperatures from the 3LM. If the noise level of the measured temperature response is higher or close to 1%, such a deviation would not produce significant differences in the final results of TIR. However, for a thickness L_i of 1 mm, the model differences increase to about 15% which would definitely change the estimation results. It can be shown, in general, that the thinner the intermediate layer, the better the approximation of the temperature evolution by 2LM. Of course, the quality of such an approximation should be estimated for every given set of parametric values.

3 Experiment

To demonstrate application of the two presented models, the laser-flash method was applied to samples composed of two metallic disks representing layers 1 and 2 and bonded by three different adhesives. The transient TIR was measured for different adhesive thicknesses and at three different temperatures.

3.1 Samples and their Properties

For the materials to be bonded, several dozens of thin polished 99.9%-pure copper disks, 1-mm thick, and 10-mm diameter were provided by Goodfellow, while for the adhesive, three different commercial types were selected; Loctite® cyanoacrylate, Bison Int. metal epoxy resin, and Henkel Co. silicon rubber.

Samples were made by joining two arbitrarily chosen copper disks with one type of adhesive. The disks were cleaned with acetone before the adhesion, and their dimensions were measured by a calibrated micrometer. The adhesion of all samples was performed at room temperature, by taking into account the curing time according to related instructions. The thickness of the cured adhesive was determined indirectly by measuring final sample dimensions.

There were, in total, nine samples: four made with cyanoacrylate with different adhesive thickness, three with metal epoxy resin, and two with silicone rubber. All the samples, related dimensions, and relative expanded uncertainties (coverage factor of two) are presented in Table 2. The uncertainties were obtained by repeated measurements, and a relatively high level of the adhesive thickness non-uniformity can be seen, while the uncertainties of the used copper disks were negligible. Although all these dimensions were measured at room temperature, they were used over the whole temperature range because the influence of the linear thermal expansion effect in comparison to the uncertainties of the adhesive layers was expected to be small.

Regarding other sample properties, they were either computed or taken from available literature data. The values of the thermal diffusivity, specific heat capacity, and density of copper were taken from Touloukian et al. [17] and Touloukian and Buyco [18], while those of the thermal linear expansion coefficient, α_i, and density of the adhesives used here are from related technical data sheets provided by producers.

Table 2 Tested samples, related dimensions, and relative expanded uncertainties

Sample code	Adhesive material	L_1(μm)	U_{L1}(%)	L_2(μm)	U_{L2} (%)	L_{i} (μm)	$U_{L\mathrm{i}}$(%)
CYA1	Cyanoacrylate	1,021	0.2	1,018	0.2	29	30.3
CYA2	Cyanoacrylate	1,021	0.2	1,017	0.2	61	14.1
CYA3	Cyanoacrylate	1,022	0.3	1,014	0.3	95	19.6
CYA4	Cyanoacrylate	1,019	0.2	1,021	0.2	150	9.7
EPO1	Epoxy resin	1,019	0.2	1,021	0.2	34	27.1
EPO2	Epoxy resin	1,039	0.2	1,021	0.3	73	21.1
EPO3	Epoxy resin	1,020	0.2	1,020	0.1	80	17.5
SIL1	Silicone rubber	1,023	0.4	1,021	0.2	72	14.2
SIL2	Silicone rubber	1,022	0.2	1,022	0.2	189	7.1

Table 3 Thermophysical properties of copper disks used in this study

T_{ref}(°C)	$a_1, a_2(10^{-4}\mathrm{m}^2\cdot\mathrm{s}^{-1})$	$\rho_1, \rho_2(\mathrm{kg}\cdot\mathrm{m}^{-3})$	$c_1, c_2\ (\mathrm{J}\cdot\mathrm{kg}^{-1}\cdot\mathrm{K}^{-1})$	$h(\mathrm{W}\cdot\mathrm{m}^{-2}\cdot\mathrm{K}^{-1})$
10	1.19	8,960	386	4.6
40	1.16	8,960	388	6.3
80	1.13	8,960	391	9.0

Table 4 Thermophysical properties of adhesives used in this study and their assumed relative expanded uncertainties

Sample code	$\rho_{\mathrm{i}}\ (\mathrm{kg}\cdot\mathrm{m}^{-3})$	$U_{\rho\mathrm{i}}$ (%)	$c_{\mathrm{i}}\ (\mathrm{J}\cdot\mathrm{kg}^{-1}\cdot\mathrm{K}^{-1})$	$U_{c\mathrm{i}}$ (%)	$\alpha_{\mathrm{i}}\ (10^{-6}\mathrm{°C}^{-1})$
CYA	1,070	5	1,500	10	80
EPO	1,200	5	1,000	15	100
SIL	1,090	5	900	15	300

The values of the specific heat capacity of the adhesives used here were taken from different sources presented in Ref. [19].

Finally, assuming only radiative heat exchange between the samples and environment (measurements under vacuum conditions), heat transfer coefficients of two free sample surfaces h_1 and h_2 were computed from an approximate formula $h \approx 4\sigma_{\mathrm{sb}}\varepsilon T_{\mathrm{ref}}^3$, where σ_{sb} is the Stefan-Boltzmann constant, T_{ref} is the sample reference temperature, and ε is the emissivity of sample surfaces. The latter property was taken to be 0.9 for both free surfaces of all samples because a thin heat conductive black carbon layer ($\sim$ 5μm) was applied to surfaces to maximize the absorption of a laser beam and to increase the temperature detection sensitivity.

All thermophysical properties of the copper disks used here for three typical reference temperatures at which the experiments were carried out are presented in Table 3, while thermophysical properties of the adhesives and their assumed uncertainties are given in Table 4.

3.2 Experimental Setup and Measurements

The laser-flash apparatus used here is described in [20]. The vacuum in the chamber was typically 3 Pa. The sample reference temperature was measured with a thin "thermocoax" K-type thermocouple positioned next to the sample lateral side.

A temperature transient is obtained by a single energy pulse from a ruby laser. The maximum output energy of the pulse was from 3 to 10 J, and the typical pulse duration was 1 ms with a relative expanded uncertainty of 10%. A liquid nitrogen-cooled InSb infrared detector was used for the detection of temperature transients. The signal from the detector was measured with a calibrated 24-bit digital multimeter. Both the data acquisition and the laser discharge were controlled and synchronized by a computer.

Experiments consisted of 81 measurements, 36 with samples bonded with cyanoacrylate, 27 with samples with epoxy resin, and 18 with silicone rubber. The sample reference temperatures were about 10, 40, and 80°C, and three signals were recorded at each reference temperature. All reference temperatures were measured with an expanded uncertainty of 0.8°C. The duration of measured transient temperatures was from 1 to 10 s, with an acquisition frequency ranging from 200 to 1,000 Hz. The maximum noise level of all recorded signals was 0.6%; the typical value was about 0.4%.

The data reduction was carried out according to the parameter estimation procedure from Sect. 2.2 for both presented models. For every signal, three estimations related to three different a priori values of the related TIR (i.e., R_c for the 2LM and a_{eff} for the 3LM, see Eqs. 7 and 8) and only one initial value of the absorbed energy were performed. These values were 10^{-5}, 10^{-4}, and $10^{-3}\,m^2\cdot K\cdot W^{-1}$ for R_c for the 2LM; 10^{-8}, 10^{-7}, and $10^{-6}\,m^2\cdot s^{-1}$ for a_{eff} for the 3LM; and $100\,J\cdot m^{-2}$ for the parameter Q for both models.

3.3 Experimental Results

The first important result of the experiments is that all parameter estimation procedures, applied to one particular signal and which correspond to one set of known parameter values, converged to a single value of the TIR, i.e., a_{eff}, independent of the initial guess. This confirms that besides the statement of the previous research [9] that the laser-flash method is very suitable for the transient TCR measurement when samples consist of two thermally conductive materials without an intermediate layer, the same estimation technique can also be applied for the transient TIR measurements of samples with an intermediate layer.

From 81 measured signals (9 signals for each sample) the averaged values of the TIR for each temperature region have been determined and they are given in Table 5 together with their relative expanded uncertainties.

It can be seen from Table 5 that the values of the transient TIR using the 2LM are higher than those estimated with the 3LM, and this difference increases with the adhesive thickness, confirming the conclusion derived in Sect. 2.3. In addition, the final uncertainties of the TIR values are much lower using the 2LM than those using the 3LM, which is also expected because of the influence of the final uncertainties of known parameters, L_i, ρ_i, and c_i. Therefore, one can conclude here that the accuracy of the transient TIR values measured by the laser-flash method depends directly on both the thickness of the intermediate layer and the knowledge of its thermophysical properties.

Table 5 Mean values of the transient TIR with related relative expanded uncertainty (coverage factor of two) for both mathematical models

Sample code	T_{ref} (°C)	2LM				3LM		
		TIR ($10^{-4}\,m^2 \cdot K \cdot W^{-1}$)	U_{TIR} (%)	k_{eff} ($W \cdot m^{-1} \cdot K^{-1}$)	U_{keff} (%)	TIR ($10^{-4}\,m^2 \cdot K \cdot W^{-1}$)	k_{eff} ($W \cdot m^{-1} \cdot K^{-1}$)	U_{TIR}, U_{keff} (%)
CYA1	11.7	1.23	0.3	0.235	35.0	1.22	0.237	11.2
	40.9	1.28	2.3	0.227	35.0	1.27	0.229	11.2
	81.7	1.26	0.7	0.231	34.9	1.25	0.233	11.2
CYA2	9.5	2.98	0.7	0.204	16.3	2.93	0.208	7.2
	38.3	2.95	0.3	0.207	16.2	2.89	0.211	7.2
	80.8	2.88	0.5	0.213	16.2	2.83	0.217	7.2
CYA3	9.0	3.97	5.4	0.239	22.6	3.86	0.246	8.7
	39.0	4.10	0.7	0.232	22.6	3.99	0.238	8.7
	78.1	4.14	1.6	0.231	22.5	4.03	0.237	8.7
CYA4	10.4	7.13	5.5	0.210	11.2	6.81	0.220	15.5
	39.7	7.46	1.1	0.201	11.2	7.14	0.211	15.5
	82.6	7.37	0.8	0.205	11.2	7.05	0.214	15.5
EPO1	10.3	0.801	2.2	0.424	15.8	0.796	0.427	15.1
	42.4	0.791	1.0	0.431	15.7	0.785	0.434	15.1
	83.3	0.795	0.4	0.431	15.7	0.788	0.434	15.1
EPO2	11.5	2.14	5.0	0.342	12.1	2.10	0.347	12.7
	42.1	2.07	1.9	0.353	12.0	2.04	0.360	12.7
	83.5	2.08	1.1	0.354	12.0	2.04	0.360	12.7
EPO3	11.8	2.22	2.3	0.359	10.1	2.19	0.366	11.2
	41.5	2.27	4.4	0.353	10.1	2.23	0.359	11.2
	83.7	2.29	2.2	0.352	10.0	2.25	0.358	11.2
SIL1	11.1	4.12	4.5	0.174	8.2	4.06	0.177	10.3
	41.9	4.00	0.5	0.181	8.2	3.94	0.184	10.3
	81.9	4.16	0.2	0.176	8.2	4.09	0.179	10.3
SIL2	11.1	10.7	5.2	0.176	4.0	10.2	0.184	8.1
	41.5	10.9	1.0	0.175	4.0	10.4	0.182	8.1
	84.7	10.7	0.5	0.180	4.0	10.2	0.189	8.1

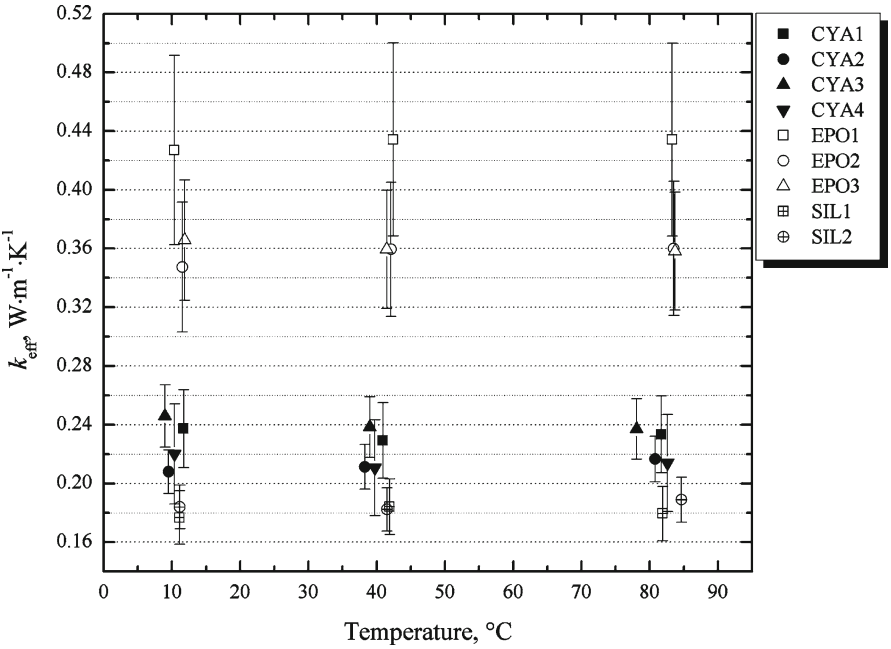

Fig. 3 Experimental results of the transient TIR of samples used in this research using the 3LM

On the other hand, to compare the experimental results, the corresponding values of the effective thermal conductivity, k_{eff}, i.e., of the inverse of the TIR multiplied by the thickness of the related adhesive layer, are also presented in Table 5, together with their expanded uncertainties. It can be seen that due to the high uncertainties of the adhesive thickness, the expanded uncertainties of the parameter k_{eff} are significantly higher than those of the TIR when the 2LM is applied, and they may be even higher than those of the k_{eff} obtained from the 3LM. It means that if the specific heat and density are accurately known or, at least, more accurately known than the thickness of the intermediate layer, the application of the 3LM in the laser-flash method gives more reliable results. On the other hand, if the thickness of the intermediate layer is thin and well defined, the use of the 2LM is recommended.

Finally, the results of the effective thermal conductivity, k_{eff}, obtained for all samples by using the 3LM are given in Fig. 3. These results show that the value of k_{eff} does not depend on the adhesive thickness but on the adhesive material as expected, and for each material, it varies within its uncertainty range. Besides, the temperature dependence of this parameter is, apparently, negligible for the applied temperature range and materials used in this research.

4 Conclusion

For measurements of the transient thermal interface resistance between two bonded metallic bodies using the laser-flash method, two mathematical models can be applied: the two-layered and three-layered model. According to performed experiments and

data reduction analysis, it can be concluded that the application of the two-layered model is recommended for thin, well defined, and uniform intermediate layers, while the three-layered model is recommended for thick intermediate layers, independent of whether they are well-defined or not. However, if the specific heat capacity and density of the intermediate layer are accurately known, the use of the three-layered model is preferred.

Appendix

Definitions of terms used in Sect. 2.1 are as follows:

$$A_n^{(2LM)} \equiv \frac{L_1}{2\varphi_{1n}}\left[\varphi_{1n}\left(1+s_{1n}^2\right)-\frac{1}{2}\sin 2\varphi_{1n}\left(1-s_{1n}^2\right)+s_{1n}\left(1-\cos 2\varphi_{1n}\right)\right] + \frac{L_2}{2\varphi_{2n}}\frac{k_1}{k_2}\left[\varphi_{2n}\left(1+s_{2n}^2\right)-\frac{1}{2}\sin 2\varphi_{2n}\left(1-s_{2n}^2\right) - s_{2n}\left(1-\cos 2\varphi_{2n}\right)\right] \tag{A1}$$

$$s_{1n} \equiv \frac{k_1\varphi_{1n}\cos\varphi_{1n}+L_1h_1\sin\varphi_{1n}}{k_1\varphi_{1n}\sin\varphi_{1n}-L_1h_1\cos\varphi_{1n}} \tag{A2}$$

$$s_{2n} \equiv \frac{k_2\varphi_{2n}\cos\varphi_{2n}+L_2h_2\sin\varphi_{2n}}{-k_2\varphi_{2n}\sin\varphi_{1n}+L_2h_2\cos\varphi_{2n}} \tag{A3}$$

$$\varphi_{1n} \equiv \frac{\beta_n L_1}{\sqrt{a_1}}, \quad \varphi_{2n} \equiv \frac{\beta_n L_2}{\sqrt{a_2}} \tag{A4}$$

$$d_1 \equiv \frac{k_1}{L_1}\varphi_{01}\cot\varphi_{01}+h_1 \tag{A5}$$

$$d_2 \equiv \frac{k_1}{L_1}\varphi_{01}\cot\varphi_{01}+\frac{1}{R_c}-\frac{1}{d_1}\left(\frac{k_1}{L_1}\frac{\varphi_{01}}{\sin\varphi_{01}}\right)^2 \tag{A6}$$

$$d_3 \equiv \frac{k_2}{L_2}\varphi_{02}\cot\varphi_{02}+\frac{1}{R_c}-\frac{1}{d_2R_c^2} \tag{A7}$$

$$d_4 \equiv \frac{k_2}{L_2}\varphi_{02}\cot\varphi_{02}+h_2-\frac{1}{d_3}\left(\frac{k_2}{L_2}\frac{\varphi_{02}}{\sin\varphi_{02}}\right)^2 \tag{A8}$$

$$\varphi_{01} \equiv \frac{\beta_0 L_1}{\sqrt{a_1}}, \quad \varphi_{02} \equiv \frac{\beta_0 L_2}{\sqrt{a_2}} \tag{A9}$$

$$\begin{aligned} A_n^{(3\mathrm{LM})} \equiv\ & \rho_1 c_1 L_1 \left[1 + p_{1n}^2 - \frac{1}{2\varphi_{1n}}\left(1 - p_{1n}^2\right)\sin 2\varphi_{1n} - \frac{1}{\varphi_{1n}} p_{1n}\left(1 - \cos 2\varphi_{1n}\right)\right] \\ & + \rho_\mathrm{i} c_\mathrm{i} L_\mathrm{i} \left[p_{3n}^2 + p_{2n}^2 + \frac{1}{2\varphi_\mathrm{i} n}\left(p_{3n}^2 - p_{2n}^2\right)\sin 2\varphi_{\mathrm{i}n}\right. \\ & \left. + \frac{1}{\varphi_{\mathrm{i}n}} p_{3n} p_{2n}\left(1 - \cos 2\varphi_{\mathrm{i}n}\right)\right] + \rho_2 c_2 L_2 \left\{\left(1 + \frac{L_\mathrm{i}}{L_2}\right)\left(1 + p_{4n}^2\right) p_{5n}^2\right. \\ & - \frac{1}{2\varphi_{2n}}\left(1 - p_{4n}^2\right) p_{5n}^2 \left[\sin 2\left(\varphi'_{\mathrm{i}n} + \varphi_{2n}\right) - \sin 2\varphi'_{\mathrm{i}n}\right] + \\ & \left. - \frac{1}{\varphi_{2n}} p_{4n} p_{5n}^2 \left[\cos 2\left(\varphi'_{\mathrm{i}n} + \varphi_{2n}\right) - \cos 2\varphi'_{\mathrm{i}n}\right]\right\} \end{aligned} \tag{A10}$$

$$p_{1n} \equiv -\frac{k_1 \varphi_{1n} \cos\varphi_{1n} + L_1 h_1 \sin\varphi_{1n}}{k_1 \varphi_{1n} \sin\varphi_{1n} - L_1 h_1 \cos\varphi_{1n}} \tag{A11}$$

$$p_{2n} \equiv \frac{k_1}{k_\mathrm{i}}\sqrt{\frac{a_\mathrm{i}}{a_1}} \tag{A12}$$

$$p_{3n} \equiv \frac{k_1 R_{c1}}{L_1}\varphi_{1n} + p_{1n} \tag{A13}$$

$$p_{4n} \equiv \frac{k_2 \varphi_{2n} \cos\left(\varphi'_{\mathrm{i}n} + \varphi_{2n}\right) + L_2 h_2 \sin\left(\varphi'_{\mathrm{i}n} + \varphi_{2n}\right)}{k_2 \varphi_{2n} \sin\left(\varphi'_{\mathrm{i}n} + \varphi_{2n}\right) - L_2 h_2 \cos\left(\varphi'_{\mathrm{i}n} + \varphi_{2n}\right)} \tag{A14}$$

$$\begin{aligned} p_{5n} \equiv\ & p_{2n} \frac{\sin\varphi_{\mathrm{i}n}}{\sin\varphi'_{\mathrm{i}n}}\left(1 + \cot^2\varphi_{\mathrm{i}n}\right) \\ & \times \left[1 + \frac{k_2 R_{c2}}{L_2}\varphi_{2n} p_{4n} - \frac{k_2}{k_\mathrm{i}}\frac{L_\mathrm{i}}{L_2}\frac{\varphi_{2n}}{\varphi_{\mathrm{i}n}} p_{4n}\right. \\ & \left. \cot\varphi_{\mathrm{i}n} - \left(\frac{k_2 R_{c2}}{L_2}\varphi_{2n} - \frac{k_2}{k_\mathrm{i}}\frac{L_\mathrm{i}}{L_2}\frac{\varphi_{2n}}{\varphi_{\mathrm{i}n}}\cot\varphi_{\mathrm{i}n} - p_{4n}\right)\cot\varphi'_{\mathrm{i}n}\right]^{-1} \end{aligned} \tag{A15}$$

$$\varphi_{\mathrm{i}n} \equiv \frac{\beta_n L_\mathrm{i}}{\sqrt{a_\mathrm{i}}}, \quad \varphi'_{\mathrm{i}n} \equiv \varphi_{\mathrm{i}n}\sqrt{\frac{a_\mathrm{i}}{a_2}} \tag{A16}$$

$$g_1 \equiv \frac{k_1}{L_1}\varphi_{01}\cot\varphi_{01} + h_1 \tag{A17}$$

$$g_2 \equiv \frac{k_1}{L_1}\varphi_{01}\cot\varphi_{01} + \frac{1}{R_{c1}} - \frac{1}{g_1}\left(\frac{k_1}{L_1}\frac{\varphi_{01}}{\sin\varphi_{01}}\right)^2 \tag{A18}$$

$$g_3 \equiv \frac{k_i}{L_i}\varphi_{0i}\cot\varphi_{0i} + \frac{1}{R_{c1}} - \frac{1}{g_2 R_{c1}^2} \tag{A19}$$

$$g_4 \equiv \frac{k_i}{L_i}\varphi_{0i}\cot\varphi_{0i} + \frac{1}{R_{c2}} - \frac{1}{g_3}\left(\frac{k_i}{L_i}\frac{\varphi_{0i}}{\sin\varphi_{0i}}\right)^2 \tag{A20}$$

$$g_5 \equiv \frac{k_2}{L_2}\varphi_{02}\cot\varphi_{02} + \frac{1}{R_{c2}} - \frac{1}{g_4 R_{c2}^2} \tag{A21}$$

$$g_6 \equiv \frac{k_2}{L_2}\varphi_{02}\cot\varphi_{02} + h_2 - \frac{1}{g_5}\left(\frac{k_2}{L_2}\frac{\varphi_{02}}{\sin\varphi_{02}}\right)^2 \tag{A22}$$

$$\varphi_{0i} \equiv \frac{\beta_0 L_i}{\sqrt{a_i}} \tag{A23}$$

References

1. E. Gmelin, M. Asen-Palmer, M. Reuther, R. Villar, J. Phys. D: Appl. Phys. **32**, R19 (1999)
2. W.J. Parker, R.J. Jenkins, C.P. Butler, G.L. Abbott, J. Appl. Phys. **32**, 1679 (1961)
3. M. Laurent, J.L. Macqueron, A. Gery, G. Sinicki, C.R.A.S. Paris **B273**, 1369 (1967) [in French]
4. A. Degiovanni, A. Gery, M. Laurent, G. Sinicki, Entropie **11**, 35 (1975) [in French]
5. H.J. Lee, Ph. D. Thesis, Purdue University, West Lafayette, Indiana, 1975
6. K. Inoue, E. Ohmura, Trans. JWRI (Japanese Welding Research Institute) **15**, 193 (1986)
7. L. Dusza, High Temp. High Press. **27/28**, 475 (1995/1996)
8. A. Griesinger, K. Spindler, E. Hahne, in *Proc. 11th IHTC*, vol. 4, Kyongju, Korea (1998), p. 101
9. N.D. Milošević, M. Raynaud, K.D. Maglić, Inverse Probl. Eng. **10**, 85 (2002)
10. R.C. Campbell, S.E. Smith, R.L. Dietz, in *Proceedings of 15th IEEE SEMI-THERM Symp.*, San Diego (1999), p. 83
11. D.P.H. Hasselman, K.Y. Donaldson, F.D. Barlow, A.A. Elshabini, G.H. Schiroky, J.P. Yaskoff, R.L. Dietz, IEEE T. Compon. Pack. Technol. **23**, 633 (2000)
12. J.G. Bai, Z.Z. Zhang, G.-O. Lu, D.P.H. Hasselman, Int. J. Thermophys. **26**, 1607 (2005)
13. H.S. Carslaw, J.C. Jaeger, *Conduction of Heat in Solids* (Clarendon Press, Oxford, 1959), pp. 319–326
14. M.N. Özişik, *Boundary Value Problems of Heat Conduction* (Int. Textbook Co., Scranton, Pennsylvania, 1968), pp. 262–298
15. M.D. Mikhailov, N.L. Vulchanov, J. Comp. Phys. **50**, 323 (1983)
16. J.V. Beck, K.J. Arnold, *Parameter Estimation in Engineering and Sciences* (Wiley, New York, 1977), pp. 340–361

17. Y.S. Touloukian, R.W. Powell, C.Y. Ho, M.C. Nikolaou, *Thermophysical Properties of Matter, The TPRL Data Series*, vol. 10, *Thermal Diffusivity* (IFI/Plenum, New York, Washington, 1973), pp. 51–61
18. Y.S. Touloukian, E.H. Buyco, *Thermophysical Properties of Matter, The TPRL Data Series*, vol. 4, *Specific Heat, Metallic Elements and Alloys* (IFI/Plenum, New York, Washington, 1970), pp. 51–61
19. www.matweb.com
20. K.D. Maglić, A. Cezairliyan, V.E. Peletsky, *Compendium of Thermophysical Property Measurement Methods*, vol. 2, *Recommended Measurement Techniques and Practices* (Plenum, New York, 1992), pp. 281–313